IOP Publishing New J. Phys. 24 (2023) 123044 https://doi.org/10.1088/1367-2630/acae3c

New Journal of Physics
The open access journal at the forefront of physics

Deutsche Physikalische Gesellschaft DPG
IOP Institute of Physics

Published in partnership with: Deutsche Physikalische Gesellschaft and the Institute of Physics

OPEN ACCESS

RECEIVED
22 June 2022

REVISED
2 December 2022

ACCEPTED FOR PUBLICATION
23 December 2022

PUBLISHED
4 January 2023

PAPER

Rotational mirror–mirror entanglement via dissipative atomic reservoir in a double-Laguerre–Gaussian-cavity system

Fei Wang[1,*], **Kang Shen**[2] **and Jun Xu**[2]

[1] School of Science, Hubei University of Technology, Wuhan 430068, People's Republic of China
[2] College of Physical Science and Technology, Central China Normal University, Wuhan 430079, People's Republic of China
[*] Author to whom any correspondence should be addressed.

E-mail: feiwang@hbut.edu.cn

Keywords: dissipation, orbital angular momentum, macroscopic entanglement

Abstract

We propose a new scheme to prepare macroscopic entanglement between two rotating mirrors using dissipative atomic reservoir in a double-Laguerre–Gaussian-cavity system. The two-level atomic system driven by a strong field, acts as a single pathway of Bogoliubov dissipation to push the two original cavity modes into the desirable entangled state under the near-resonant conditions. Successively, the photon–photon entanglement can be transferred to mirror–mirror entanglement through the exchange of orbital angular momentum. In essence, the macroscopic entanglement is originated from the dissipative atomic reservoir rather than the radiation torque, thereby it is usually robust against environmental noises. The present scheme provides a feasible way to realize stable entanglement between spatially separated mirrors with high capacity, which may find potential applications in remote quantum communications.

1. Introduction

In recent years, the interaction between structured light beams and matter has been paid continuous attention in quantum optics and quantum information. Particularly, the Laguerre–Gaussian (LG) beam, as a typical type of structured light, can be obtained by solving the paraxial wave equation in cylindrical coordinates, possessing a helical wavefront and a doughnut-shaped intensity distribution with a hollow at the beam center [1, 2]. The LG beam usually carries an orbital angular momentum (OAM) of $l\hbar$ per photon with its phase of $e^{il\phi}$, where l is topological charge value and ϕ represents azimuthal angle [3]. In experiment, the typical methods to generate LG light are spatial light modulators [4, 5], spiral phase plate or mirror [6, 7] and computer-generated holograms [8, 9]. It is demonstrated that the topological charge value l can reach as high as 1000 by using the spiral phase plate [10]. Interestingly, the LG beams can exert a torque on objects due to the exchange of OAM [11–13], with which it is possible to trap and cool the rotational mirrors [14]. So far, a large number of quantum optics phenomena have been reported based on the interaction of LG light with matter, including the vortex light information storage [15], quantum memory [16], spatially dependent electromagnetically induced transparency [17], transfer of optical vortices via the multi-wave mixing [18–21], optomechanical induced transparency [22], ground-state cooling [23], the detection of OAM [24], the generation of higher order sideband [25, 26], and the high-dimensional quantum entanglement [27–34] etc.

On the other hand, the macroscopic entanglement is of great importance both in verifying the fundamental quantum theory [35] and realizing realistic applications such as remote quantum communication, reliable quantum computation, precision measurement and quantum sensing [36, 37] etc. In experiment, the entanglement between two macroscopic objects is demonstrated by engineering the dissipation with laser and magnetic fields [38]. The mechanical resonator at the micrometer scale, an ideal candidate for investigating macroscopic entanglement, has attracted much attention in last years because it locates at the interface of the quantum-to-classical transition [39–44]. It is explored that the macroscopic oscillators can be entangled by using the radiation pressure, behind which both the parametric interaction

and beam splitter interaction are hidden [45]. Successively, various literatures focus on the methods to entangle two massive, movable cavity mirrors at steady state [46–49]. As a profitable model, the bipartite and multipartite entanglement between mirrors and cavity modes are also acquired under the effect of radiation pressure force [50, 51]. Interestingly, it provides a useful way to control the macroscopic entanglement by atomic coherence effects [52–56], in which the parametric interaction between mechanical oscillators is established by the coherence-controlled evolution processes. A lot of recent studies show that the hybrid quantum systems have developed an extensive platform to generate macroscopic entanglement between distant objects [57–60], which may find potential applications in remote quantum communications.

Notably, in a rotational optomechanical system, Bhattacharya opens up fascinating possibilities, in their pioneering works, to entangle a LG cavity mode and a rotating mirror [61], or generate entanglement between the rovibrational modes of a macroscopic mirror using radiation pressure [62]. Motivated by this device, Chen *et al* report the macroscopic entanglement between two rotating mirrors through the exchange of OAM with the same LG cavity [63]. Later, by placing a yttrium iron garnet (YIG) sphere into the LG cavity, the tripartite entanglement are generated between cavity mode, mirror and magnon [64]. While the YIG sphere is replaced by a two-level atomic ensemble, the cavity–mirror entanglement and quantum coherence are enhanced by choosing suitable parameters [65], which is attributed to the fact that the effective coupling of the parametric interaction is enhanced by injecting the atoms. Nevertheless, the quantum coherence would be spoiled when the large detuning limit is not satisfied. In addition, they point out that the quantum coherence are also significantly suppressed by the large atomic decay.

In this paper, we present a different way to establish macroscopic entanglement between two spatially separate rotating mirror via a single pathway of Bogoliubov dissipation. The main results we find in the present scheme are listed as follows. First, in dressed-state picture, it is seen that the two original modes constitute a pair of Bogoliubov modes, one of which mediates into the interaction while the other 'dark mode' is decoupled with the system. When the dissipation process is dominant over the amplification process, the Bogoliubov mode would evolve into a squeezed vacuum state, causing the generation of entanglement. This entangled state is successively transferred to two rotating mirrors via the beam splitter interaction. Obviously, the macroscopic entanglement is essentially originated from dissipation rather than radiation torque. Second, we find that the optimal macroscopic entanglement can be obtained when the driving field is nearly resonant with the atomic transition. There exists two extreme cases where the entanglement is vanished. At the exact resonant condition, the entanglement disappears since the dissipation rate is negligible when the dressed-state populations are identical. For the large detuning cases, the entanglement is also significantly suppressed due to the reduction squeezing parameter. Therefore, the best entanglement is obtained at an appropriate value of driving detuning. Third, we note that the macroscopic entanglement can be obtained when the damping rates of the atoms are much larger than the cavity losses, i.e. $\gamma \gg \kappa$. As a result, the atomic system can be viewed as a reservoir and the treatment of adiabatically eliminating atomic variables is valid. We extract the atomic contribution of the dissipative reservoir effects clearly and the quantum noises from atoms are included to calculate the quantum entanglement. Our results explore that the atomic damping rates have positive effects on macroscopic entanglement, which is completely different from the schemes in [65]. Finally, comparing with previous schemes [61–65], the macroscopic entanglement can be simply controlled by the strength and detuning of the driving field on atoms, which may provide conveniences for experimental implement.

The remaining part of the present paper is organized as follows. In section 2, we describe the system model of the double-Laguerre–Gaussian-cavity (DLGC) system. The master equation and Heisenberg–Langevin equations for the cavity modes and rotating mirrors are derived. In section 3 we present the physical mechanisms and discuss the numerical results of the remote mirror–mirror entanglement with two different methods. Finally, the conclusion is given in section 4.

2. Model and equations

The rotational DLGC system under consideration is presented in figure 1(a), in which the system consists of two fixed mirrors ($FM_{1,2}$) and two rotational mirrors ($RM_{1,2}$). We consider that a two-level atomic ensemble is placed at the cross site of the two cavities. The RM mirrors are mounted on the support points $S_{1,2}$ and can rotate around the axis $Z_{1,2}$, respectively. Without loss of generality, we assume that the fixed mirrors $FM_{1,2}$ are partially transparent while $RM_{1,2}$ have perfect reflection. When the LG beams $G_{1,2}$ with 0 charge are incident on $FM_{1,2}$, we only consider the transmitted beams with unchanged 0 charge since the reflected components do not interact with the atomic ensemble. The two 0 charge beams reflected from the $RM_{1,2}$ can get charged to $+2l_{1,2}$. It has been explored in experiment that LG beams can exert a torque on microscopic particles, in which the optical vortices are generated [13]. In addition, Bhattacharya and Meystre *et al* use OAM transfer from a LG beam to trap and cool the rotational motion of a macroscopic mirror made of a

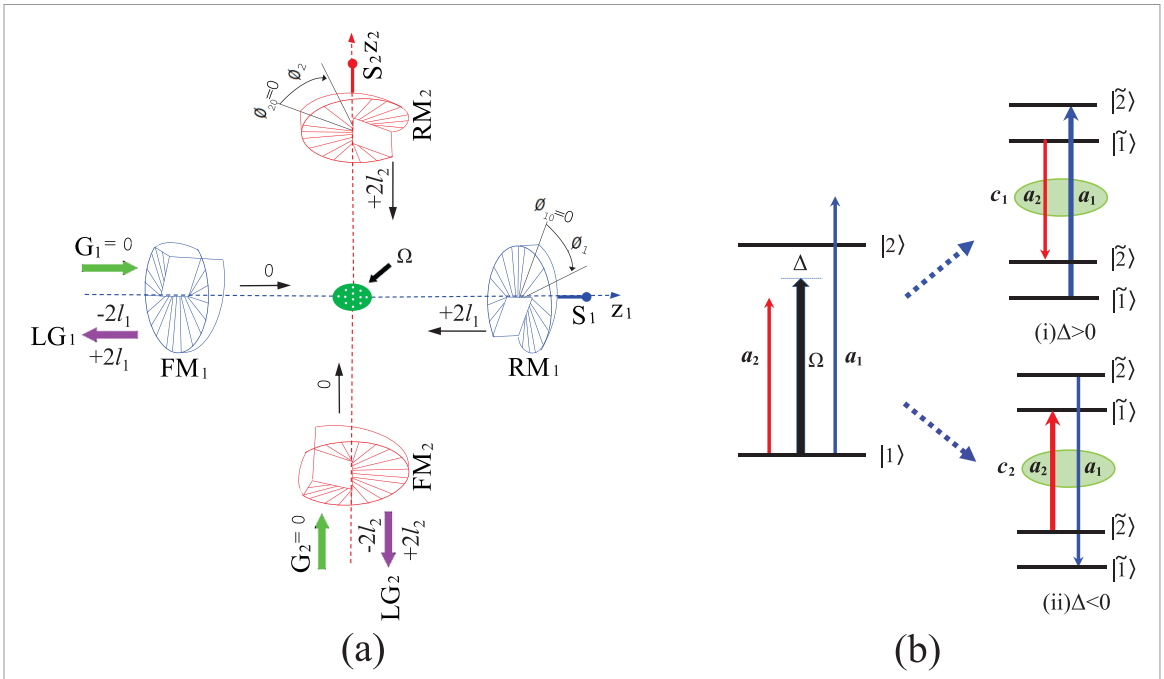

Figure 1. (a) Schematic diagram of DLGC system. The system consists of two fixed mirrors ($FM_{1,2}$) and two rotating mirrors ($RM_{1,2}$). A two-level atomic ensemble driven by strong field Ω is placed at the intersection of the two cavities. The RM mirrors are mounted on the support points $S_{1,2}$ and can rotate around the axis $Z_{1,2}$, respectively. We assume that the fixed mirrors $FM_{1,2}$ are partially transparent while $RM_{1,2}$ have perfect reflection. (b) The energy level structure of the two-level atomic system, in which Ω is the Rabi frequency and Δ represents the atomic detuning. The two cavity fields denoted by annihilation operators $a_{1,2}$ couple to the common atomic transition with different cavity detunings. For $\Delta > 0$, the original modes $a_{1,2}$ are resonant with the Rabi sidebands and they constitute a Bogoliubov mode c_1 to mediate into the interaction. In the other case of $\Delta < 0$, c_1 is replaced by the other Bogoliubov mode c_2 to interact with the atomic system.

perfectly reflecting spiral phase element [14]. Assuming both RMs have the same mass m and radius r_0, their moments of inertia about the axis $Z_{1,2}$ passing through the center are $I_{1,2} = mr_0^2/2$. The $RM_{1,2}$ oscillate like two pendulums with angular frequencies $\omega_{\phi_{1,2}}$. Notably, the $RM_{1,2}$ act as two harmonic oscillators for the angular deviations $\phi_{1,2} \ll 2\pi$ and they have the equilibrium position $\phi_{10,20} = 0$. Apart from the internal spin angular moment ($\ll \hbar$), photons in LG beams carry integral OAM numbers $\hbar l_{1,2}$, respectively [2]. Therefore, when the LG beams are incident on the cavity, they can transfer torques $\hbar\xi_{\phi_j} = cl_j\hbar/L_j (j = 1, 2)$ per photon to the $RM_{1,2}$, in which c represents the velocity of light and $L_{1,2}$ are the length of the two cavities. Then the mechanical effects of the LG beams interacting with the macroscopic rotating mirrors should be considered. The Hamiltonians of the DLGC system plus the atomic ensemble are written as ($\hbar = 1$)

$$H_0 = \omega_{21}\sigma_{22} - \frac{\Omega}{2}(\sigma_{12}e^{i\omega_0 t} + \sigma_{21}e^{-i\omega_0 t}), \tag{1}$$

$$H_1 = \sum_{j=1}^{2}\left[\nu_j a_j^\dagger a_j + (g_j a_j \sigma_{21} + g_j a_j^\dagger \sigma_{12})\right], \tag{2}$$

$$H_2 = \sum_{j=1}^{2}\left[\frac{L_{z_j}^2}{2I_j} + \frac{1}{2}I_j\omega_{\phi_j}^2\phi_j^2 - \xi_{\phi_j}a_j^\dagger a_j\phi_j + i(\varepsilon_j a_j^\dagger e^{-i\omega_{L_j}} - \varepsilon_j^* a_j e^{i\omega_{L_j}})\right], \tag{3}$$

wherein H_0 represents the system Hamiltonian for the two-level atoms driven by a strong field with frequency ω_0 and Rabi frequency Ω. The atomic transition frequency is denoted by ω_{21}. $\sigma_{lm} = \sum_{\mu=1}^{N}|l_\mu\rangle\langle m_\mu|(l, m = 1, 2)$ are the projection operators of N independent atoms for $l = m$ and the flip operators for $l \neq m$. H_1 describes the free Hamiltonian of the two cavity modes plus the interaction Hamiltonian between the atoms and cavity modes with coupling constants $g_j (j = 1, 2)$. $a_j(a_j^\dagger)$ are the annihilation (creation) operators for the two cavity modes with the frequencies ν_j. H_2 denotes the free Hamiltonians of the two rotational cavity mirrors, the interaction between the cavity modes and two rotating mirrors, the driving Hamiltonian to the cavity modes by the external laser fields with frequencies ω_{L_j} and the amplitudes of $|\varepsilon_j| = \sqrt{2P_j\kappa_j/\hbar\omega_{L_j}}$, wherein κ_j are the cavity damping rates and P_j input power of the laser.

L_{z_j} are the angular momentum of RM about the axis with the commutation relation $[L_{z_j}, \phi_k] = -i\hbar\delta_{jk}(j,k=1,2)$. According to [14], we can define

$$\phi_j = \sqrt{\frac{\hbar}{2I_j\omega_{\phi_j}}}(b_j^\dagger + b_j), \tag{4}$$
$$L_{z_j} = i\sqrt{\frac{\hbar I_j\omega_{\phi_j}}{2}}(b_j^\dagger - b_j),$$

in which the annihilation and creation operators for the rotating mirrors are denoted by b_j and $b_j^\dagger$, respectively. Substituting the above expression into equation (3), making a unitary transform with $U = \exp(-iH^{'}t)$ and $H^{'} = \omega_0(a_1^\dagger a_1 + a_2^\dagger a_2 + \sigma_{22})$, we can rewrite the Hamiltonian H_0 and H_1 as

$$\tilde{H}_0 = \Delta\sigma_{22} - \frac{\Omega}{2}(\sigma_{12} + \sigma_{21}), \tag{5}$$

$$\tilde{H}_1 = \sum_{j=1}^{2}[\Delta_{c_j}a_j^\dagger a_j + (g_j a_j\sigma_{21} + g_j a_j^\dagger\sigma_{12})], \tag{6}$$

$$\tilde{H}_2 = \sum_{j=1}^{2}[\omega_{\phi_j}b_j^\dagger b_j - G_j a_j^\dagger a_j(b_j^\dagger + b_j) + i\varepsilon_j(a_j^\dagger e^{-i\delta_j t} - a_j e^{i\delta_j t})], \tag{7}$$

where $\Delta_{c_j} = \nu_j - \omega_0$, $\Delta = \omega_{21} - \omega_0$, $\delta_j = \omega_{L_j} - \omega_0$ are cavity detunings, atomic detunings and driving detunings, respectively. The coupling parameters G_j are defined as $G_j = \frac{cl_j}{L_j}\sqrt{\frac{\hbar}{2I\omega_{\phi_j}}}(j=1,2)$.

The atomic relaxation, the cavity losses and the intrinsic damping rates of rotating mirrors are taken the forms as

$$\mathcal{L}_a\rho = \frac{\gamma}{2}(2\sigma_{12}\rho\sigma_{21} - \sigma_{21}\sigma_{12}\rho - \rho\sigma_{21}\sigma_{12}), \tag{8}$$

$$\mathcal{L}_c\rho = \sum_{j=1,2}\frac{\kappa_j}{2}(2a_j\rho a_j^\dagger - \rho a_j^\dagger a_j - a_j^\dagger a_j\rho), \tag{9}$$

$$\mathcal{L}_b\rho = \sum_{j=1,2}\frac{\gamma_{\phi_j}}{2}(2b_j\rho b_j^\dagger - \rho b_j^\dagger b_j - b_j^\dagger b_j\rho). \tag{10}$$

To obtain the reduced master equation of cavity modes, as proposed in [66], we resort to the dressed atomic picture by diagonalizing the Hamiltonian $\tilde{H}_0$ under the conditions of $|\Omega| \gg \gamma, \kappa_j, g_j$. The dressed atomic states are expressed in terms of bare states as [67]

$$|\tilde{1}\rangle = \cos\theta|1\rangle - \sin\theta|2\rangle, \tag{11}$$
$$|\tilde{2}\rangle = \sin\theta|1\rangle + \cos\theta|2\rangle,$$

in which $\cos\theta = \sqrt{\frac{1}{2} + \frac{d}{2\sqrt{1+d^2}}}$ and $\sin\theta = \sqrt{\frac{1}{2} - \frac{d}{2\sqrt{1+d^2}}}$ with normalized detuning $d = \frac{\Delta}{\Omega}$. The dressed states $|\tilde{1}\rangle$ and $|\tilde{2}\rangle$ have their eigenvalues $\lambda_{1,2} = \frac{1}{2}(\Delta \mp \tilde{\Omega})$ with $\tilde{\Omega} = \sqrt{\Delta^2 + \Omega^2}$, respectively. Now the system Hamiltonian of $\tilde{H}_0$ is rewritten in the dressed-state picture as $H_d = \sum_j \lambda_j\sigma_{\tilde{j}\tilde{j}}(j=1,2)$. By transforming the bare atomic relaxation term (8) into the dressed-state picture and neglecting the quantized mods temporarily, the steady-state populations of the dressed states $N_j = \langle\sigma_{\tilde{j}\tilde{j}}\rangle(j=1,2)$ are obtained as

$$N_1 = \frac{N\cos^4\theta}{\cos^4\theta + \sin^4\theta}, \quad N_2 = \frac{N\sin^4\theta}{\cos^4\theta + \sin^4\theta}. \tag{12}$$

Clearly, for $\Delta = 0$, we have $\sin\theta = \cos\theta = \frac{1}{2}$ and $N_1 = N_2 = \frac{N}{2}$, namely, the populations of the two dressed states are identical at the exact resonant condition. For $\Delta \neq 0$, we have $N_1 > N_2$ (or $N_1 < N_2$) when $\Delta > 0$ (or $\Delta < 0$). The equilibrium is broken and then the dissipative atomic reservoir effect is possible [68]. Making a further unitary transformation with $U^{'} = \exp(-iH_d t)$ on the Hamiltonian $\tilde{H}_1$, the effective Hamiltonian is derived as

$$H_{\text{eff}} = (g_1\cos^2\theta a_1 - g_2\sin^2\theta a_2^\dagger)\sigma_{\tilde{2}\tilde{1}} + \text{H.c.}, \tag{13}$$

in which we take the conditions of $\Delta_{c_1} = -\Delta_{c_2} = \tilde{\Omega}$, i.e. the cavities are tuned to be resonant with the Rabi sidebands. If the cavity detunings are tuned to be comparable to or larger than the level spacing $\tilde{\Omega}$, the effective Hamiltonian is no longer valid. Under the good-cavity limit of $\gamma \gg \kappa_j (j = 1, 2)$, the atomic variable can be adiabatically eliminated using the standard quantum optics techniques [69, 70]

$$\dot{\rho}_c = -i\mathrm{Tr}_a[H_{\mathrm{eff}}, \rho_c] + \mathcal{L}_c\rho_c. \tag{14}$$

Finally, the reduced master equation of the cavity modes takes the form

$$\begin{aligned}\dot{\rho}_c = {} & A_1(a_1\rho_c a_1^\dagger - \rho_c a_1^\dagger a_1) + A_2(a_2\rho_c a_2^\dagger - \rho_c a_2^\dagger a_2) \\ & + B_1(a_1^\dagger\rho_c a_1 - \rho_c a_1 a_1^\dagger) + B_2(a_2^\dagger\rho_c a_2 - \rho_c a_2 a_2^\dagger) \\ & - C_1(a_1\rho_c a_2 - \rho_c a_2 a_1) - C_2(a_2\rho_c a_1 - \rho_c a_1 a_2) \\ & - C_1(a_2^\dagger\rho_c a_1^\dagger - \rho_c a_1^\dagger a_2^\dagger) - C_2(a_1^\dagger\rho_c a_2^\dagger - \rho_c a_1^\dagger a_2^\dagger) + \mathrm{H.c.},\end{aligned} \tag{15}$$

where the parameters are $A_j = (n_j + 1)\kappa_j + N_j\xi_j$, $B_j = n_j\kappa_j + N_{3-j}\xi_j$, and $C_j = N_j\sqrt{\xi_1\xi_2}$ $(j = 1, 2)$ with the coefficients $\xi_1 = 2g_1^2\cos^4\theta/(\gamma + \gamma_c)$, $\xi_2 = 2g_2^2\sin^4\theta/(\gamma + \gamma_c)$, $\gamma_c = \gamma\sin^2 2\theta/2$. Here n_j represent the mean thermal photon number of the cavities.

In present scheme, we focus on investigating macroscopic entanglement between two rotating mirrors. To do so, we make use of reduced master equation (15) and the Hamiltonian $\tilde{H}_2$ to obtain the dynamics equation as

$$\begin{aligned}\dot{a}_1 &= -(\kappa_{a_1} - i\omega_1)a_1 + \chi a_2^\dagger + \varepsilon_1 e^{-i\delta_1 t} + F_1, \\ \dot{a}_2 &= -(\kappa_{a_2} - i\omega_2)a_2 - \chi a_1^\dagger + \varepsilon_2 e^{-i\delta_2 t} + F_2, \\ \dot{b}_j &= -(\gamma_{\phi_j} + i\omega_{\phi_j})b_j + iG_j a_j^\dagger a_j + \sqrt{2\gamma_{\phi_j}}F_{b_j}.\end{aligned} \tag{16}$$

For simplicity, we define $\kappa_{a_1} = \kappa_1 - (N_2 - N_1)\xi_1$, $\kappa_{a_2} = \kappa_2 + (N_2 - N_1)\xi_2$, $\omega_j = G_j\langle b_j + b_j^\dagger\rangle (j = 1, 2)$, $\chi = C_1 - C_2$. F_j are noise operators including the cavity losses and the atomic contribution part. F_{b_j} represent the mechanical noise operators coupling to the rotating mirrors from the thermal environment. Without loss of generality, we have vanishing mean $\langle F_x(t)\rangle = 0$ and the nonzero second order correlation terms $\langle F_x(t)F_y(t')\rangle = 2D_{xy}\delta(t - t')$ as

$$\begin{aligned}&\langle F_j(t)F_j^\dagger(t')\rangle = 2A_j\delta(t - t'), \quad \langle F_j^\dagger(t)F_j(t')\rangle = 2B_j\delta(t - t'), \\ &\langle F_1(t)F_2(t')\rangle = 2C_1\delta(t - t'), \quad \langle F_2(t)F_1(t')\rangle = 2C_2\delta(t - t'), \\ &\langle F_{b_j}^\dagger(t')F_{b_j}(t)\rangle = n_{\phi_j}\delta(t - t'), \quad \langle F_{b_j}(t)F_{b_j}^\dagger(t')\rangle = (n_{\phi_j} + 1)\delta(t - t'),\end{aligned} \tag{17}$$

wherein $n_{\phi_j} = [\exp\frac{\hbar\omega_{\phi_j}}{k_B T_j} - 1]^{-1}$ is the mean occupation number, k_B is the Boltzmann constant and T_j the environmental temperature of the mechanical resonator.

According to equation (16), by defining $a_j = \tilde{a}_j e^{-i\delta_j t}$, we can neglect the the highly oscillating terms for $\delta_1 + \delta_2 \gg 1$ and then the steady-state solutions for $\langle\tilde{a}_j\rangle$ and $\langle b_j\rangle$ are derived as

$$\begin{aligned}\langle\tilde{a}_j\rangle &= \frac{\varepsilon_j}{\kappa_{a_j} - i(\delta_j + \omega_j)}, \\ \langle b_j\rangle &= \frac{(\omega_{\phi_j} + i\gamma_{\phi_j})G_j}{\gamma_{\phi_j}^2 + \omega_{\phi_j}^2}\langle a_j^\dagger a_j\rangle.\end{aligned} \tag{18}$$

The equation for the intracavity mean photon numbers is given by

$$I_{a_j}[\kappa_{a_j}^2 + (\delta_j + \eta_j I_{a_j})^2] = |\varepsilon_j|^2, \tag{19}$$

in which we define $\eta_j = 2\omega_{\phi_j}G_j/(\gamma_{\phi_j}^2 + \omega_{\phi_j}^2)$, $I_{a_j} = \langle a_j^\dagger a_j\rangle = \langle\tilde{a}_j^\dagger\tilde{a}_j\rangle$. It is clear that the two rotating mirrors will exhibit optical bistable behavior and experience strong nonlinearities, which can be controlled by the detuning and strength of the driving field on atoms.

To explore the macroscopic entanglement between two rotating mirrors, we can linearize the equation (16) around the semiclassical state corresponding to a working point in the stable range, i.e. $\hat{o} = \langle\hat{o}_s\rangle + \delta\hat{o}$. The steady state solutions $\langle\hat{o}_s\rangle$ are given in equation (18) and $\delta\hat{o}$ represents the quantum fluctuation around the mean value. Furthermore, we introduce the slowly varying fluctuation operators $\delta a_j = \delta\tilde{a}_j e^{-i\delta_j t}$ and $b_j = \tilde{b}_j e^{-i\omega_{\phi_j} t}$. By dropping the high-frequency oscillating terms $\exp[-i(\delta_1 + \delta_2)t]$ at

$\delta_j = \omega_{\phi_j}$, the corresponding linear quantum Langevin equations for the quantum fluctuations are obtained as

$$\begin{aligned}
\delta\dot{a}_1 &= -(\kappa_{a_1} - i\omega_1)\delta a_1 + \chi\delta a_2^\dagger + i\tilde{g}_1\delta\tilde{b}_1 + F_1,\\
\delta\dot{a}_2 &= -(\kappa_{a_2} - i\omega_2)\delta a_2 - \chi\delta a_1^\dagger + i\tilde{g}_2\delta\tilde{b}_2 + F_2,\\
\delta\dot{\tilde{b}}_j &= -\gamma_{\phi_j}\delta\tilde{b}_j + i\tilde{g}_j^*\delta a_j + \tilde{F}_{b_j},
\end{aligned} \tag{20}$$

wherein $\tilde{F}_{b_j} = \sqrt{2\gamma_{\phi_j}}F_{b_j}e^{i\omega_{\phi_j}t}$, $\tilde{g}_j = G_j\langle\tilde{a}_j\rangle (j = 1, 2)$. Then the quantum entanglement between the two mirrors can be calculated and discussed according to the above equations, which will be presented in the following section.

3. Analysis and discussion

In this section, we would like to elucidate the mechanism for the generation of rotational optomechanical entanglement. Next, the numerical results of mirror–mirror entanglement are presented by nonadiabatical eliminating and adiabatical eliminating of cavities, respectively. The possible experimental parameters are briefly discussed in the last subsection.

3.1. Physical mechanism analysis

3.1.1. Dissipation of cavity fields in light of Bogoliubov modes

In order to describe the internal mechanisms for the generation of quantum entanglement more clearly, we define a pair of Bogoliubov modes in equation (13) for the cavity fields: $c_1 = a_1\cosh r - a_2^\dagger\sinh r$, $c_2 = a_2\cosh r - a_1^\dagger\sinh r$ with the squeezing parameter $\tanh r = \tan^2\theta$ for $\Delta > 0$ and $\tanh r = \cot^2\theta$ for $\Delta < 0$. The interaction between the dressed atoms and the Bogoliubov mode is shown in figure 1(b). Correspondingly, the system Hamiltonian of equation (13) is simply rewritten as

$$\begin{aligned}
\tilde{H}_{\rm eff} &= G_{\rm eff}(c_1\sigma_{\tilde{2}\tilde{1}} + \sigma_{\tilde{1}\tilde{2}}c_1^\dagger) \quad \text{for} \quad \Delta > 0,\\
\tilde{H}_{\rm eff} &= -G_{\rm eff}(c_2^\dagger\sigma_{\tilde{2}\tilde{1}} + \sigma_{\tilde{1}\tilde{2}}c_2) \quad \text{for} \quad \Delta < 0,
\end{aligned} \tag{21}$$

where the effective coupling constant $G_{\rm eff} = g\sqrt{|\cos 2\theta|}$ by assuming $g_1 = g_2 = g$. Note that only the collective mode c_1 (or c_2) mediates into the interaction while the other mode c_2 (or c_1) is decoupled with the system for the two cases. This is termed as a single pathway of Bogoliubov dissipation, which can lead to the occurrence of quantum entanglement [66, 68]. Under the adiabatic elimination conditions of $\gamma \gg \kappa_{1,2}$, we can obtain the atomic contribution part of the reduced master equation for the Bogoliubov mode $c_{1,2}$ as

$$\begin{aligned}
\dot{\rho}_{c_1} &= \mathcal{A}_1(2c_1\rho c_1^\dagger - c_1^\dagger c_1\rho - \rho c_1^\dagger c_1) + \mathcal{B}_1(2c_1^\dagger\rho c_1 - c_1c_1^\dagger\rho - \rho c_1c_1^\dagger) \quad \text{for} \quad \Delta > 0,\\
\dot{\rho}_{c_2} &= \mathcal{A}_2(2c_2\rho c_2^\dagger - c_2^\dagger c_2\rho - \rho c_2^\dagger c_2) + \mathcal{B}_2(2c_2^\dagger\rho c_2 - c_2c_2^\dagger\rho - \rho c_2c_2^\dagger) \quad \text{for} \quad \Delta < 0,
\end{aligned} \tag{22}$$

in which $\mathcal{A}_1 = \mathcal{B}_2 = 2G_{\rm eff}^2N_1/\Gamma$ and $\mathcal{A}_2 = \mathcal{B}_1 = 2G_{\rm eff}^2N_2/\Gamma$ with $\Gamma = \frac{\gamma}{2} + \frac{\gamma}{4}\sin^2 2\theta$. It is seen that the $\mathcal{A}$ terms represent the dissipation and the $\mathcal{B}$ terms denote the excitation of Bogouliubov modes, respectively. When dissipation rate $\mathcal{R} = \mathcal{A} - \mathcal{B} \gg \kappa$, the Bogoliubov mode c_1 (or c_2) will evolve into the squeezed vacuum state while the other mode c_2 (or c_1) is decoupled with the system. Generally, the larger the dissipation rate is, the stronger the entanglement will be. For $\Delta = 0$, we have $N_1 = N_2$ and $\mathcal{R} = 0$, leading to the absence of quantum entanglement, which is verified by the following numerical calculations. However, when the normalized detuning d deviates slightly away from the resonant conditions, we have $\mathcal{R} \gg \kappa$ in the positive ($\Delta > 0$) and negative frequency regions ($\Delta < 0$) due to $N_1 \neq N_2$, thus resulting in the appearance of entanglement. For example, at $d = 0.3$, we have $N_1/N = 0.77$, $N_2/N = 0.23$ and $\mathcal{R} = 1.7\gamma \gg \kappa$, meaning that the adiabatical elimination of atomic variables and the single-pathway dissipation of Bogoliubov are valid. On the other hand, the entanglement is simultaneously determined by the squeezing parameter r. When d is increased, the squeezing parameter r is inversely decreased accompanying by the increasing of the dissipation rate $\mathcal{R}$. For example, the squeezing parameter ($\tanh r = \tan^2\theta$) is $r = 1.15$ at $d = 0.1$, $r = 0.41$ at $d = 0.5$, and $r = 0.17$ at $d = 1$. As a consequence, the best entanglement appears at the near-resonant conditions when the dissipation rate and the squeezing parameter r have a compatible value.

3.1.2. Entangled state transfer from cavity fields to rotating mirrors

Next, we would like to clarify the frequency arrangement of the present system. As shown in figure 2(a), on the one hand, the cavity fields $a_{1,2}$ are tuned to be resonant with the sidebands, i.e. $\nu_j = \omega_0 \pm \tilde{\Omega}$. For the cavity detunings $\Delta_{c_1} = -\Delta_{c_1} = \tilde{\Omega}$, we have $\nu_j - \Delta_{c_j} = \omega_0$. On the other hand, it is seen that the frequencies

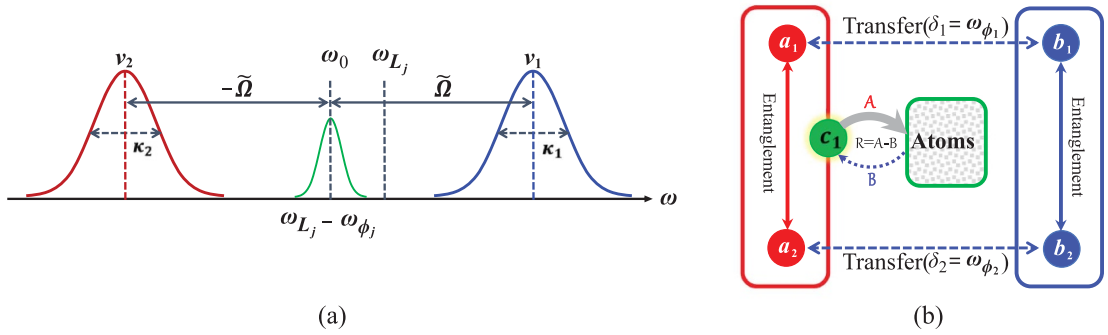

Figure 2. (a) The demonstration of frequency arrangement for the cavity modes, rotating mirrors and driving fields. It is seen that the frequencies for the drive fields satisfy the relations of $\omega_{L_j}-\omega_{\phi_j}=\omega_0$. The two cavity modes are tuned to be resonant with the red sideband and blue sideband $\nu_j=\omega\pm\tilde{\Omega}$, respectively. (b) Schematic demonstration for the rotating mirror-mirror entanglement in the case of $\Delta>0$. The two original modes $a_{1,2}$ constitute a pair of Bogoliubov modes $c_{1,2}$ to mediate into the interaction with dressed atoms. For $\Delta<0$, the collective mode c_1 is replaced by c_2 as shown in equation (21). When the dissipation coefficient is larger than the gain coefficient, $\mathcal{A}>\mathcal{B}$, the collective mode c_1 will evolve into a squeezed vacuum state while the mode c_2 (not shown) is decoupled with the system, giving rise to the entanglement between two modes $a_{1,2}$. Successively, the entangled state is transferred to the macroscopic mirrors via transfer and cooling processes at $\delta_j=\omega_{\phi_j}(j=1,2)$.

of the rotating mirrors ω_{ϕ_j} and the frequencies of driving fields on cavities $\omega_{L_j}(j=1,2)$ satisfy the relations of $\omega_{L_j}-\omega_{\phi_j}=\omega_0$. Due to the driving detunings $\delta_j=\omega_{L_j}-\omega_0$, we have the relations of $\delta_j=\omega_{\phi_j}$, giving rise to that the high-frequency oscillating terms $\exp[-i(\delta_1+\delta_2)]$ in equation (20) should be dropped. Obviously, these terms with the form of $\tilde{g}_j(\delta a_j\delta b_j+\delta a_j^\dagger\delta b_j^\dagger)$ describing parametric amplification are absent while the terms of $\tilde{g}_j(\delta a_j\delta b_j^\dagger+\delta a_j^\dagger\delta b_j)(j=1,2)$ being responsible for quantum state transfer are existent [71]. In addition, as shown in figure 2(b), the internal physical mechanisms for the generation of macroscopic entanglement are depicted in detail. For $\Delta>0$, two original modes $a_{1,2}$ constitute a pair of collective modes $c_{1,2}$, in which the 'bright mode' c_1 would dissipate into the atomic reservoir for $\mathcal{R}>0$ while the other 'dark mode' c_2 (not shown) is decoupled with the system. As a result, the bipartite photon–photon entanglement is essentially established by the atomic reservoir effects and then it is transferred to two macroscopic rotating mirrors at $\delta_j=\omega_{\phi_j}$ via the two transfer processes $a_j\leftrightsquigarrow b_j$. Finally, it is worthwhile to point out that the present system is completely different from the previous schemes proposed in [65]. In their works, the two-level atomic ensemble or magnon is placed into the cavity to enhance the cavity–mirror entanglement or to realize the tripartite entanglement based on the parametric interaction.

3.2. Rotating mirror–mirror entanglement without adiabatic elimination of cavities

In the first of place, we assume that the cavity modes are not adiabatically eliminated. To numerically calculate the quantum correlations between the two rotating mirrors, two pairs of quadrature operators are defined as $\delta x_j=(\delta a_j+\delta a_j^\dagger)/\sqrt{2}$, $\delta p_j=-i(\delta a_j-\delta a_j^\dagger)/\sqrt{2}$, $\delta\phi_j=(\delta\tilde{b}_j+\delta\tilde{b}_j^\dagger)/\sqrt{2}$, $\delta L_j=-i(\delta\tilde{b}_j-\delta\tilde{b}_j^\dagger)/\sqrt{2}$. Then we can write the dynamical equations of quantum fluctuations in a concise form

$$\dot{\vec{u}}=M\vec{u}(t)+\vec{F}(t), \tag{23}$$

where $\vec{u}(t)=(\delta x_1,\delta p_1,\delta x_2,\delta p_2,\delta\phi_1,\delta L_1,\delta\phi_2,\delta L_2)^T$, $\vec{F}(t)=(F_{x_1},F_{p_1},F_{x_2},F_{p_2},F_{\phi_1},F_{L_1},F_{\phi_2},F_{L_2})^T$. The corresponding composite noise operators are written as $F_{x_j}=(F_j+F_j^\dagger)/\sqrt{2}$, $F_{p_j}=-i(F_j-F_j^\dagger)/\sqrt{2}$, $F_{\phi_j}=(\tilde{F}_{b_j}+\tilde{F}_{b_j}^\dagger)/\sqrt{2}$, $F_{L_j}=-i(\tilde{F}_{b_j}-\tilde{F}_{b_j}^\dagger)/\sqrt{2}$. The drift matrix M takes the form

$$\begin{pmatrix}
-\kappa_{a_1} & -\omega_1 & \chi & 0 & -\mu_1 & \mu_2 & 0 & 0\\
\omega_1 & -\kappa_{a_1} & 0 & -\chi & \mu_2 & -\mu_1 & 0 & 0\\
-\chi & 0 & -\kappa_{a_2} & -\omega_2 & 0 & 0 & -\mu_3 & \mu_4\\
0 & \chi & \omega_2 & -\kappa_{a_2} & 0 & 0 & \mu_4 & -\mu_3\\
-\mu_1 & \mu_2 & 0 & 0 & -\gamma_{\phi_1} & 0 & 0 & 0\\
\mu_2 & -\mu_1 & 0 & 0 & 0 & -\gamma_{\phi_1} & 0 & 0\\
0 & 0 & -\mu_3 & \mu_4 & 0 & 0 & -\gamma_{\phi_2} & 0\\
0 & 0 & \mu_4 & -\mu_3 & 0 & 0 & 0 & -\gamma_{\phi_2}
\end{pmatrix}, \tag{24}$$

where in $\mu_1=\mathrm{Im}\tilde{g}_1$, $\mu_2=\mathrm{Re}\tilde{g}_1$, $\mu_3=\mathrm{Im}\tilde{g}_2$, $\mu_4=\mathrm{Re}\tilde{g}_2$. Generally, the system would be stable if the real parts of all eigenvalues of M are negative, which can be judged based on numerical calculation in the present scheme [72]. Throughout this paper, we always guarantee that the system is stable via choosing appropriate

Table 1. The possible experimental parameters.

Number	Parameter	Description	Value
1	L	Cavity length	0.245 mm
2	λ	Laser wavelength	810 nm
3	$\omega_{\phi_{1,2}}$	Rotating mirror frequencies	∼MHz
4	m	Rotating mirror mass	100 ng
5	r_0	Rotating mirror radius	10 μm
6	γ	Spontaneous decay rate of atom	$2\pi \times 5$ MHz
7	$\kappa_{1,2}$	Decay rates of cavity modes	$2\pi \times 0.5$ MHz
8	Q	Quality factor of rotating mirrors	$10^6 \sim 10^7$
9	$g_{1,2}$	Coupling constants	∼MHz

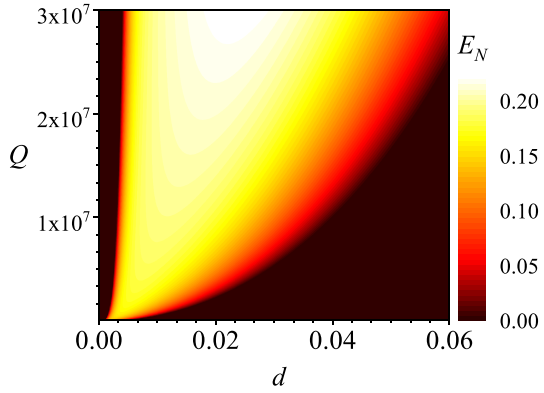

Figure 3. The logarithmic negativity E_N is plotted as a function of the normalized detuning d and the cavity quality factor Q for $l_1 = l_2 = 40$, $\omega_{\phi_1} = 2\pi \times 1$ MHz and $\omega_{\phi_2} = 2\pi \times 10$ MHz. The other parameters are chosen as those in table 1.

system parameters. When the stability conditions are fulfilled, the steady-state Lyapunov equation is given by [50]

$$MV + MV^T = -D, \tag{25}$$

in which D denotes the diffusion matrix and V is a 8×8 covariance matrix (CM) with the matrix elements of $V_{ij} = \frac{1}{2}[\langle u_i(\infty)u_j(\infty)\rangle + \langle u_j(\infty)u_i(\infty)\rangle]$. The CM of two modes is taken the form as

$$V = \begin{pmatrix} V_1 & V_3 \\ V_3^T & V_2 \end{pmatrix}, \tag{26}$$

wherein the matrix V_1, V_2 and V_3 are the 2×2 submatrices. The diffusion matrix D are defined as $D_{ij}\delta(t-t') = \langle F_i(t)F_j(t') + F_j(t')F_i(t)\rangle/2$ and the nonzero diffusion coefficients are $D_{11} = D_{22} = A_1 + B_1$, $D_{33} = D_{44} = A_2 + B_2$, $D_{55} = D_{66} = \gamma_{\phi_1}(2n_{\phi_1} + 1)$, $D_{77} = D_{88} = \gamma_{\phi_2}(2n_{\phi_2} + 1)$, $D_{13} = D_{31} = -D_{24} = -D_{42} = C_1 + C_2$.

Once the CM of the system is achieved, one can calculate the degree of the mirror-mirror entanglement. We adopt a reliable logarithmic negativity criterion to study continuous variable quantum entanglement for Gaussian states [73, 74]. The definition of E_N is given by

$$E_N = \max[0, -\ln 2\Lambda], \tag{27}$$

where $\Lambda = 2^{-1/2}[\Sigma - \sqrt{\Sigma^2 - 4\det V}]^{1/2}$ with $\Sigma = \det V_1 + \det V_2 - 2\det V_3$.

In the following numerical calculations, the possible experimental parameters are listed in table 1 as proposed in [14, 61, 62]. In figure 3, the evolution of logarithmic negativity E_N is plotted versus the normalized detuning d and quality factor Q of cavities by choosing the OAM as $l_1 = l_2 = 40$. The angular frequencies of rotating mirrors are $\omega_{\phi_1} = 2\pi \times 1$ MHz and $\omega_{\phi_2} = 2\pi \times 10$ MHz. The cavity-atom coupling constants are always set as $g_1 = g_2 = 2\pi \times 8.8$ MHz. It is found that the entanglement first increases to a maximal value and then decreases slowly to zero in the positive frequency region. At this time, the entanglement disappears in the negative frequency domain because the stability condition is not satisfied when $\omega_{\phi_1} < \omega_{\phi_2}$. On the contrary, the stability condition would be satisfied in the region of $d < 0$ for $\omega_{\phi_1} > \omega_{\phi_2}$. Specially, at $d = 0$, as shown in equation (22), the gain coefficients $\mathcal{B}_j$ are equal to the absorption

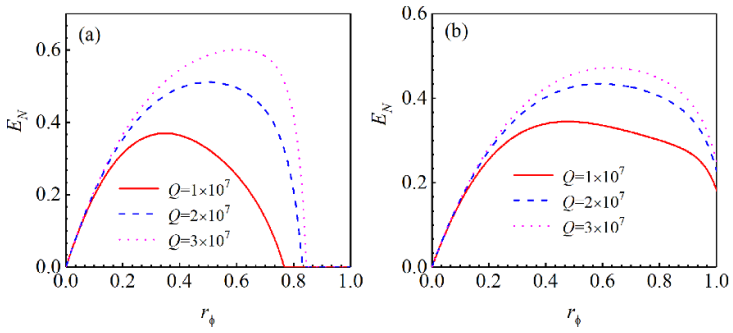

Figure 4. The logarithmic negativity E_N is plotted as a function of the angular frequency ratio r_ϕ for two cases: (a)$l_1 = l_2$; (b) $l_1 \neq l_2$; We choose the parameters as $\omega_{\phi_2} = 2\pi \times 10$ MHz, $d = 0.012$, $P_1 = P_2 = 100$ mW, $Q = 1 \times 10^7$ (solid line), 2×10^7 (dashed line), 3×10^7 (dotted line), respectively. The other parameters are chosen as those in table 1.

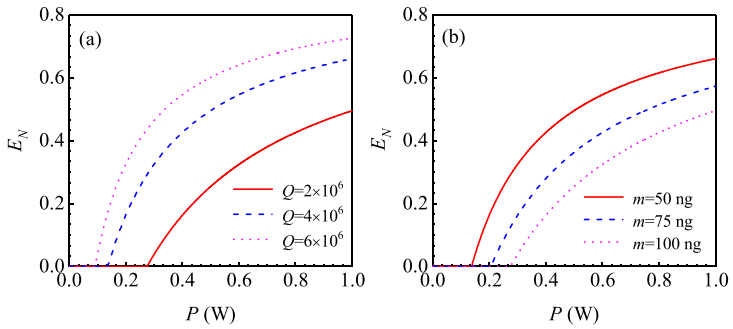

Figure 5. (a) The dependence of logarithmic negativity E_N on the input power $P_1 = P_2 = P$ by choosing different quality factor $Q_1 = Q_2 = 2 \times 10^6$ (solid line); 4×10^6 (dashed line); 6×10^6 (dotted line). (b) The evolution of logarithmic negativity E_N versus input power by choosing different masses of rotating mirrors $m_1 = m_2 = m = 50$ ng (solid line), 75 ng (dashed line), 100 ng (dotted line). The OAM is chosen as $l_1 = l_2 = 40$ and the other parameters are the same as those in table 1.

coefficients $\mathcal{A}_j (j = 1, 2)$ for $N_1 = N_2$, yielding the disappearance of mirror–mirror entanglement together with the single-pathway dissipation. Differently, with the increasing of normalized detuning d, the best entanglement happens at an appropriate value of d. Besides, we notice that the entanglement is remarkably enhanced and the entanglement region becomes wide with high quality factor Q.

In figure 4, the logarithmic negativity E_N is plotted as a function of the angular frequency ratio of $r_\phi = \omega_{\phi_1}/\omega_{\phi_2}$ for two cases: (a) $l_1 = l_2 = 40$; (b) $l_1 = 40, l_2 = 46$ by choosing different quality factor $Q = 1 \times 10^7$ (solid line), $Q = 2 \times 10^7$ (dashed line), $Q = 3 \times 10^7$ (dotted line), respectively. The normalized detuning d is chosen as $d = 0.012$ and the input powers are $P_1 = P_2 = 100$ mW. From these figures, it is found that the variation trend of E_N is similar to that in figure 3. Notably, at $r_\phi = 1$, the entanglement vanishes for $l_1 = l_2$ while occurs for $l_1 \neq l_2$, which can be attributed to that there is no exchange of total orbital angular moment between the cavity modes and rotating mirrors since the system is totally symmetrical [63]. Such a balance is broken for $l_1 \neq l_2$, leading to the generation of quantum entanglement at $r_\phi = 1$.

Next, we plot the entanglement evolution of E_N versus the input power $P = P_1 = P_2$. The other parameters are chosen as $l_1 = l_2 = 40$, $\omega_{\phi_1} = 2\pi \times 10$ MHz, $\omega_{\phi_2} = 2\pi \times 6$ MHz. In figure 5(a), logarithmic negativity E_N is plotted by choosing different quality factor $Q = 2 \times 10^6$ (solid line), 4×10^6 (dashed line), 6×10^6 (dotted line) and the influence of the rotating mirror masses on quantum entanglement is shown in figure 5(b) by choosing $m_1 = m_2 = m = 50$ ng (solid line), 75 ng (dashed line), 100 ng (dotted line) for $Q = 2 \times 10^6$, respectively. As seen from figure 5(a), we have $P_{\text{th}} = 274$ mW at $Q = 2 \times 10^6$, $P_{\text{th}} = 135$ mW at $Q = 4 \times 10^6$ and $P_{\text{th}} = 91$ mW at $Q = 6 \times 10^6$. Obviously, the larger the quality factor is, the smaller the threshold power P_{th} will be. From figure 5(b), the threshold power P_{th} is changed from 136 mW, 205 mW to 271 mW when the mirror masses are increased from 50 ng to 100 ng, demonstrating that the macroscopic quantum effects are modified by the system parameters including mirror mass m, cavity length L and the mirror radius r_0 etc.

The density plot of logarithmic negativity E_N versus the OAM l and the normalized detuning d is shown in figure 6(a) and the two-dimensional curves are plotted in figure 6(b) by setting $l = l_1 = l_2$. The parameters are chosen as $\omega_{\phi_1} = 2\pi \times 10$ MHz, $\omega_{\phi_2} = 2\pi \times 6$ MHz, $\gamma = 2\pi \times 20$ MHz, $Q = 2 \times 10^7$ and the mirror masses are chosen as $m_1 = m_2 = 50$ ng. As shown in figure 6(a), when the absolute value of $|d|$ is increased,

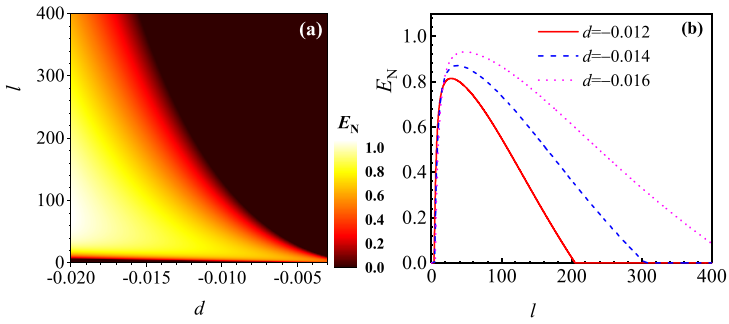

Figure 6. The logarithmic negativity E_N is plotted as a function of the OAM $l_1 = l_2 = l$ and the normalized detuning d. The other parameters are chosen as those in table 1.

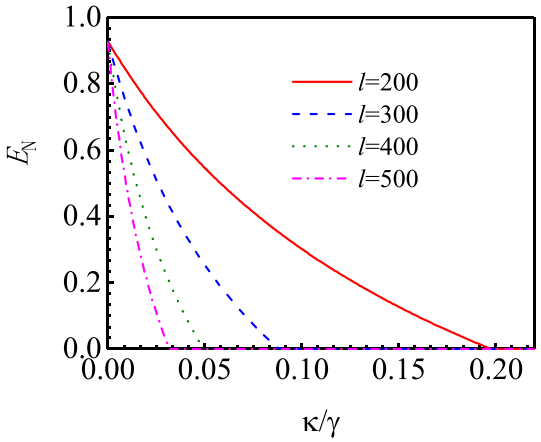

Figure 7. The evolution of logarithmic negativity E_N versus κ/γ by choosing different OAM numbers $l = 200$ (solid line), 300 (dashed line), 400 (dotted line), 500 (dash dotted line) with $l_1 = l_2 = l$, the normalized detuning $d = -0.014$, $m = 10$ ng, $Q_1 = Q_2 = 2 \times 10^7$, $r_1 = r_2 = 5\,\mu$m. The other parameters are chosen as those in table 1.

the entanglement appears and the region for $E_N > 0$ becomes wide. To show this characteristic more clearly, the two-dimensional curves of the logarithmic negativity E_N are plotted in figure 6(b) by choosing different normalized detuning d. It is seen that the best entanglement appears at an appropriate value of l, which can be used to detect topological charge value via the measurement of quantum entanglement.

Figure 7 shows the evolution of logarithmic negativity E_N as a function of κ/γ by choosing different OAM numbers of l for $\kappa_1 = \kappa_2 = \kappa$. It is clear that the good entanglement is obtained under the conditions of $\gamma \gg \kappa$. With the increasing of κ/γ, the values of logarithmic negativity E_N are monotonously decreased to zero at a specific value of κ/γ. By changing l from 200 to 500, the entanglement disappears at $\kappa/\gamma = 0.2$, 0.088, 0.05, 0.03, respectively. When the cavity losses are comparable to the atomic damping rates, the entanglement would be vanished, which is different from the results presented in [65]. What's more, the effects of thermal noise on quantum entanglement are also discussed in figure 8. The parameters are the same as those in figure 6(b) except for $d = -0.014$. As shown in figures 8(a) and (b), we find that the entanglement is relatively robust against environmental noise although it becomes worse as the thermal occupation numbers of $n_{\phi_{1,2}}$ and $n_{1,2}$ increase.

3.3. Rotating mirror–mirror entanglement with adiabatic elimination of cavities

Usually, the damping rates of the rotating mirrors are much smaller than the cavity losses, i.e. $\gamma_\phi \ll \kappa_j$. Then we derive the fluctuations dynamical equations for the two rotating mirrors by adiabatically eliminating cavities as

$$\begin{aligned} \delta\dot{\tilde{b}}_1 &= -\alpha_1\delta\tilde{b}_1 + \beta_1\delta\tilde{b}_2^\dagger + F'_{b_1}, \\ \delta\dot{\tilde{b}}_2 &= -\alpha_2\delta\tilde{b}_2 - \beta_2\delta\tilde{b}_1^\dagger + F'_{b_2}, \end{aligned} \tag{28}$$

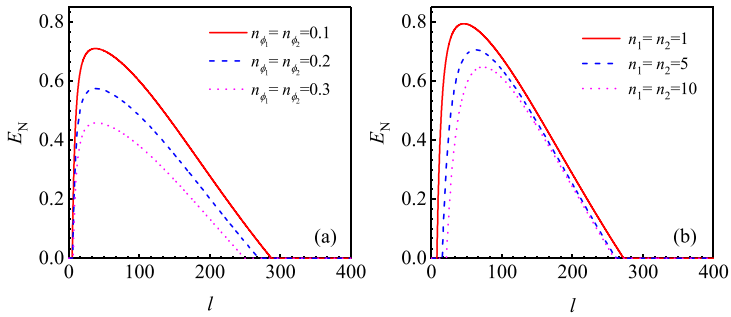

Figure 8. (a) The evolution of logarithmic negativity E_N versus the orbital momentum angular l by choosing different phonon numbers of $n_{\phi_{1,2}}$ in (a) and different thermal photon numbers of n in (b). The other parameters are the same as those in figure 6(b).

where the parameters $\alpha_1 = \gamma_{\phi_1} - |\tilde{g}_1|^2(\kappa_{a_2} - i\tilde{g}_2)/\Theta^*$, $\alpha_2 = \gamma_{\phi_2} - |\tilde{g}_2|^2(\kappa_{a_1} - i\omega_1)/\Theta$, $\beta_1 = \beta_2^* = \tilde{g}_1\tilde{g}_2\xi_{12}/\Theta^*$ with $\Theta = (\kappa_{a_1} - i\omega_1)(\kappa_{a_2} + i\omega_2) + \xi_{12}^2$, $\xi_{12} = \xi_1 - \xi_2$. The noise operators are given by

$$F'_{b_1} = -u_{11}F_1^\dagger - u_{12}F_2 + \sqrt{2\gamma_{\phi_1}}\tilde{F}_{b_1}$$
$$F'_{b_2} = u_{21}F_1 - u_{22}F_2^\dagger + \sqrt{2\gamma_{\phi_2}}\tilde{F}_{b_2}, \tag{29}$$

in which we have the coefficients $u_{11} = -i\tilde{g}_1(\kappa_{a_2} - i\omega_2)/\Theta^*$, $u_{12} = i\tilde{g}_1\xi_{12}/\Theta^*$, $u_{21} = i\tilde{g}_2\xi_{12}/\Theta$ and $u_{22} = -i\tilde{g}_2(\kappa_{a_1} - i\omega_1)/\Theta$. From the equation (28), it is seen that the parametric interaction is hidden behind the effective Hamiltonian of the two rotating mirrors. This can be used to explain the physical origin of the remote mirror–mirror entanglement. It is worthwhile to point out that the parametric interaction arises from the two-photon process in dissipative atomic reservoir effects rather than the exchange of OAM. Interestingly, as show in equation (29), we find that the dissipation effects of the present system are determined by the following four factors: the atomic decay rate γ, the thermal noise of the mechanical oscillators γ_{ϕ_j}, the cavity dissipation κ_j and the coherent-controlled dissipative atomic reservoir effect. Being different from the previous work [52–54], we find that the dissipative atomic reservoir plays an important role in generating rotating mirror–mirror entanglement, which may find potential applications in remote quantum communications.

In order to verify the validity of the adiabatic elimination approach, we follow the same procedure as in the preceding subsection to investigate the mirror–mirror entanglement with the same criterion. The dynamical equations of the quantum fluctuations of the rotating mirrors are written in a concise form as

$$\dot{\vec{u}}'(t) = M'\vec{u}'(t) + \vec{F}'(t), \tag{30}$$

in which the column vectors $\vec{u}'(t) = (\delta\phi_1, \delta L_1, \delta\phi_2, \delta L_2)^T$, $\vec{F}'(t) = (F'_{\phi_1}, F'_{L_1}, F'_{\phi_2}, F'_{L_2})^T$ and the drift matrix M' is derived as

$$M' = \begin{pmatrix} -\alpha_{11} & \alpha_{12} & \beta_{11} & \beta_{12} \\ -\alpha_{12} & -\alpha_{11} & \beta_{12} & -\beta_{11} \\ -\beta_{22} & -\beta_{21} & -\alpha_{22} & \alpha_{21} \\ -\beta_{21} & \beta_{22} & -\alpha_{21} & -\alpha_{22} \end{pmatrix}, \tag{31}$$

where $\alpha_{11} = \mathrm{Re}\alpha_1$, $\alpha_{22} = \mathrm{Re}\alpha_2$, $\alpha_{12} = \mathrm{Im}\alpha_1$, $\alpha_{21} = \mathrm{Im}\alpha_2$, $\beta_{11} = \mathrm{Re}\beta_1$, $\beta_{22} = \mathrm{Re}\beta_2$, $\beta_{12} = \mathrm{Im}\beta_1$ and $\beta_{21} = \mathrm{Im}\beta_2$. The quadrature noise operators are defined as $F'_{\phi_j} = (F_{b'_j} + F^\dagger_{b'_j})/\sqrt{2}$ and $F'_{L_j} = (F_{b'_j} - F^\dagger_{b'_j})/\sqrt{2}i$. According to Lyapunov equation, we can calculate the quantum correlations between two mirrors numerically. Notably, the nonzero diffusion coefficients can be calculated based on equation (29). For simplicity, the cumbersome expression of the diffusion matrix is not presented here.

In figure 9, we plot the logarithmic negativity E_N versus the input power and OAM for adiabatical and nonadiabatical elimination cases. The parameters are chosen as $\omega_{\phi_1} = 2\pi \times 10$ MHz, $\omega_{\phi_2} = 2\pi \times 6$ MHz, $d = -0.014$, $\gamma = 2\pi \times 20$ MHz, $m_1 = m_2 = 50$ ng, $Q_1 = Q_2 = 2 \times 10^7$, $\kappa_1 = \kappa_2 = 2\pi \times 0.5$ MHz and the other parameters are the same as those in table 1. It is seen that the results of adiabatical elimination cases are in well agreement with the nonadiabatical elimination cases when the condition of $\gamma_\phi \ll \kappa_a$ is satisfied, indicating that both methods are valid for calculating the quantum entanglement.

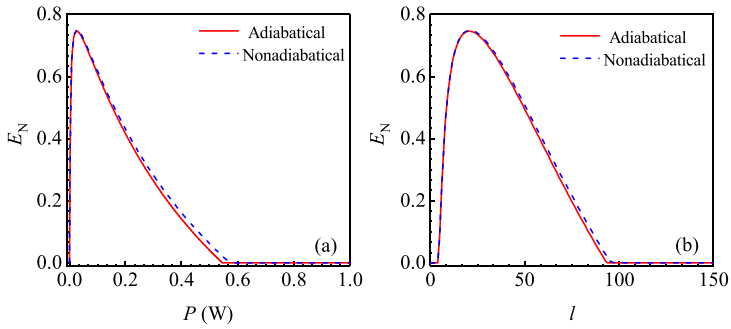

Figure 9. (a) Plots of logarithmic negativity E_N versus input power P with $l_1 = l_2 = l = 40$. (b) The evolution of logarithmic negativity E_N versus the OAM $l_1 = l_2 = l$ with $P_1 = P_2 = 100$ mW for adiabatical elimination (solid line) and nonadiabatical elimination (dashed line) cases. The parameters are chosen as $\omega_{\phi_1} = 2\pi \times 10$ MHz, $\omega_{\phi_2} = 2\pi \times 6$ MHz, $d = -0.014$, $\gamma = 2\pi \times 20$ MHz, $m_1 = m_2 = 50$ ng, $Q_1 = Q_2 = 2 \times 10^7$, $\kappa_1 = \kappa_2 = 0.1\gamma$ and the other parameters are the same as those in table 1.

3.4. Experimental implementations

Let us discuss the feasibility of the present scheme based on the current experiments. In the present scheme, the parameters of the DLGC system are chosen as proposed in previous works [14, 26, 61, 62]: $L = 0.245$ mm, $\omega_{\phi_{1,2}}$ are of the order MHz, $r_0 = 10\,\mu$m, $m = 100$ ng, $\gamma/2\pi = 5$ MHz, $\kappa_{1,2}/2\pi = 0.5$ MHz. The cavity-atom coupling constants $g_1/2\pi = g_2/2\pi = g/2\pi = 8.8$ MHz [55] and we consider the atomic ensemble with $N \sim 10^4$ atoms [75]. In experiment, the high-l LG modes can be realized via spiral phase elements and the azimuthal structure of light can be modified via reflection or transmission from the spiral phase elements [10]. It is demonstrated that high precision and low mass (sub-μg) of mirrors can be fabricated and the LG beams with a topological charge value as high as 1000 [10]. With the development of nanotechnology, the suitable spiral phase elements for the implementation of present scheme is possible to create [14, 76]. Besides, the mechanical oscillators has been experimentally reported with high quality factors ($Q \sim 10^8$), low effective mass ($m \sim 37$ pg) and high frequency (a few MHz) [77], which implies that the present scheme is feasible in experiment with current technology.

Before ending this section, we would like to emphasis the main differences between the present scheme and previous works. In the first of place, in our work, we find that the entanglement is essentially originated from the dissipative atomic reservoir and the transfer processes between cavity modes and mirrors. This is in contrast with previous schemes [64, 65], wherein the hybrid entanglement happens based on the parametric interaction under appropriate conditions, without which not only the tripartite entanglement but also the bipartite entanglement is impossible to realize. Specifically, in [65], the two-level atoms are injected into the cavity to enhance the cavity-mirror entanglement by choosing proper parameters rather than to prepare entanglement. Secondly, in our work, the single-pathway dissipation rate $\mathcal{R} = \mathcal{A} - \mathcal{B}$ and the squeezing parameter r combine to induce the mirror-mirror entanglement at the near-resonant conditions. Consequently, the conditions to generate entanglement are also distinct from those in [65], where the entanglement and quantum coherence are acquired, as expected, on the large detuning limit with low-excitation atoms. In addition, since the atomic damping rate is harmful for the quantum coherence, they consider a situation where the atomic decay rate γ is smaller than the cavity loss κ and the quantum noises of the atomic variables are neglected. Nevertheless, in the dissipative atomic reservoir scheme, the atomic variables are adiabatically eliminated under the condition of $\gamma \gg \kappa$ and the quantum noises from atoms are useful for the generation entanglement. In other words, we provide an interesting way to utilize the atomic noises instead of to combat them for preparing entanglement. Thirdly, being different from the coherent-controlled evolution processes [52–56], the macroscopic entanglement arising from dissipation, in principle, can exist for a long enough time and it is usually robust against environmental noises. Last but not least, we explore that the optimal entanglement is acquired at a specific topological charge value of l, which may find potential applications to detect topological charge via the measurement of the mirror–mirror entanglement.

4. Conclusion

In summary, the macroscopic entanglement between two rotating mirrors are theoretically investigated based on the atomic reservoir effects in a DLGC system. It is found out that the microscopic photon–photon entanglement prepared by a single pathway of Bogoliubov dissipation can be transferred to two macroscopic rotating mirrors at proper frequency conditions. We explore that the optimal entanglement is obtained when

the driving field is nearly resonant with the atomic transition and the stable entanglement is possible to obtain when the atomic decay rates are larger than the cavity losses. Finally, it turns out that two different methods with or without adiabatically elimination of cavities to calculate the mirror–mirror entanglement are equivalent. The present scheme provides a way to establish macroscopic entanglement between the mirrors without direct interaction, which may be useful for the long-distance quantum communications and quantum sensing technology.

Data availability statement

No new data were created or analysed in this study.

Acknowledgments

This work is supported by the National Natural Science Foundation of China (Grant No. 11574179) and is funded by National '111 Research Center' Microelectronics Circuits.

References

[1] Allen L, Barnett S M and Padgett M J 2016 *Optical Angular Momentum* (Bristol: Institute of physics publishing)
[2] Allen L, Beijersbergen M W, Spreeuw R J C and Woerdman J P 1992 Orbital angular momentum of light and the transformation of Laguerre-Gaussian laser modes *Phys. Rev.* A **45** 8185
[3] Yao A M and Padgett M J 2011 Orbital angular momentum: origins, behavior and applications *Adv. Opt. Photon.* **3** 161
[4] Forbes A, Dudley A and Mclaren M 2016 Creation and detection of optical modes with spatial light modulators *Adv. Opt. Photon.* **8** 200
[5] Zhu L and Wang J 2014 Arbitrary manipulation of spatial amplitude and phase using phase-only spatial light modulators *Sci. Rep.* **4** 7441
[6] Beijersbergen M W, Coerwinkel R, Kristensen M and Woerdman J P 1994 Helical-wavefront laser beams produced with a spiral phaseplate *Opt. Commun.* **112** 321
[7] Turnbull G A, Robertson D A, Smith G M, Allen L and Padgett M J 1996 The generation of free-space Laguerre-Gaussian modes at millimetre-wave frequencies by use of a spiral phaseplate *Opt. Commun.* **127** 183
[8] Heckenberg N R, McDuff R G, Smith C P and White A G 1992 Generation of optical phase singularities by computer generated hologram *Opt. Lett.* **17** 221
[9] Arlt J, Dholakia K, Allen L and Padgett M J 1999 Parametric down-conversion for light beams possessing orbital angular momentum *Phys. Rev.* A **59** 3950
[10] Shen Y, Campbell G T, Hage B, Zou H, Buchler B C and Lam P K 2013 Generation and interferometric analysis of high charge optical vortices *J. Opt.* **15** 044005
[11] He H, Friese M E J, Heckenberg N R and Rubinsztein-Dunlop H 1995 Direct observation of transfer of angular momentum to absorptive particles from a laser beam with a phase singularity *Phys. Rev. Lett.* **75** 826
[12] Andersen M F, Ryu C, Cladé P, Natarajan V, Vaziri A, Helmerson K and Phillips W D 2006 Quantized rotation of atoms from photons with orbital angular momentum *Phys. Rev. Lett.* **97** 170406
[13] Volpe G and Petrov D 2006 Torque detection using Brownian fluctuations *Phys. Rev. Lett.* **97** 210603
[14] Bhattacharya M and Meystre P 2007 Using a Laguerre-Gaussian beam to trap and cool the rotational motion of a mirror *Phys. Rev. Lett.* **99** 153603
[15] Pugatch R, Shuker M, Firstenberg O, Ron A and Davidson N 2007 Topological stability of stored optical vortices *Phys. Rev. Lett.* **98** 203601
[16] Ding D-S, Zhou Z-Y, Shi B-S and Guo G-C 2013 Single-photon-level quantum image memory based on cold atomic ensembles *Nat. Commun.* **4** 2527
[17] Radwell N, Clark T W, Piccirillo B, Barnett S M and Franke-Arnold S 2015 Spatially dependent electromagnetically induced transparency *Phys. Rev. Lett.* **114** 123603
[18] Walker G, Arnold A S and Franke-Arnold S 2012 Trans-spectral orbital angular momentum transfer via four-wave mixing in Rb vapor *Phys. Rev. Lett.* **108** 243601
[19] Zhang D, Liu X, Yang L, Li X, Zhang Z and Zhang Y 2017 Modulated vortex six-wave mixing *Opt. Lett.* **42** 3097
[20] Wang H-H, Wang J, Kang Z-H, Wang L, Gao J-Y, Chen Y and Zhang X-J 2019 Transfer of orbital angular momentum of light using electromagnetically induced transparency *Phys. Rev.* A **100** 013822
[21] Hamedi H R, Ruseckas J, Paspalakis E and Juzeliūnas G 2019 Transfer of optical vortices in coherently prepared media *Phys. Rev.* A **99** 033812
[22] Peng J-X, Chen Z, Yuan Q-Z and Feng X-L 2019 Optomechanically induced transparency in a Laguerre-Gaussian rotational-cavity system and its application to the detection of orbital angular momentum of light fields *Phys. Rev.* A **99** 043817
[23] Liu Y-M, Bai C-H, Wang D-Y, Wang T, Zheng M-H, Wang H-F, Zhu A-D and Zhang S 2018 Ground-state cooling of rotating mirror in double-Laguerre-Gaussian-cavity with atomic ensemble *Opt. Express* **26** 6143
[24] Zhang Z, Pei J, Wang Y-P and Wang X 2021 Measuring orbital angular momentum of vortex beams in optomechanics *Front. Phys.* **16** 32503
[25] Kazemi S H and Mahmoudi M 2020 Optomechanical second-order sideband effects in a Laguerre–Gaussian rotational-cavity system *Phys. Scr.* **95** 045107
[26] Xiong H, Huang Y-M and Wu Y 2021 Laguerre-Gaussian optical sum-sideband generation via orbital angular momentum exchange *Phys. Rev.* A **103** 043506
[27] Zhang W, Ding D-S, Dong M-X, Shi S, Wang K, Liu S-L, Li Y, Zhou Z-Y, Shi B-S and Guo G-C 2016 Experimental realization of entanglement in multiple degrees of freedom between two quantum memories *Nat. Commun.* **7** 13514

[28] Dada A C, Leach J, Buller G S, Padgett M J and Andersson E 2011 Experimental high-dimensional two-photon entanglement and violations of generalized Bell inequalities *Nat. Phys.* **7** 677
[29] Malik M, Erhard M, Huber M, Krenn M, Fickler R and Zeilinger A 2016 Multi-photon entanglement in high dimensions *Nat. Photon.* **10** 248
[30] Kues M *et al* 2017 On-chip generation of high-dimensional entangled quantum states and their coherent control *Nature* **546** 622
[31] Wang J *et al* 2018 Multidimensional quantum entanglement with large-scale integrated optics *Science* **360** 285
[32] Guo Y, Hu X-M, Liu B-H, Huang Y-F, Li C-F and Guo G-C 2018 Experimental witness of genuine high-dimensional entanglement *Phys. Rev.* A **97** 062309
[33] Zeng Q, Wang B, Li P and Zhang X 2018 Experimental high-dimensional Einstein-Podolsky-Rosen steering *Phys. Rev. Lett.* **120** 030401
[34] Designolle S, Srivastav V, Uola R, Valencia N H, McCutcheon W, Malik M and Brunner N 2021 Genuine high-dimensional quantum steering *Phys. Rev. Lett.* **126** 200404
[35] Schwab K C and Roukes M L 2005 Putting mechanics into quantum mechanics *Phys. Today* **58** 36
[36] Fröwis F, Sekatski P, Dür W, Gisin N and Sangouard N 2018 Macroscopic quantum states: measures, fragility and implementations *Rev. Mod. Phys.* **90** 025004
[37] Wasilewski W, Jensen K, Krauter H, Renema J J, Balabas M V and Polzik E S 2010 Quantum noise limited and entanglement-assisted magnetometry *Phys. Rev. Lett.* **104** 133601
[38] Krauter H, Muschik C A, Jensen K, Wasilewski W, Petersen J M, Cirac J I and Polzik E S 2011 Entanglement generated by dissipation and steady state entanglement of two macroscopic objects *Phys. Rev. Lett.* **107** 080503
[39] Eisert J, Plenio M B, Bose S and Hartley J 2004 Towards quantum entanglement in nanoelectromechanical devices *Phys. Rev. Lett.* **93** 190402
[40] Paz J P and Roncaglia A J 2008 Dynamics of the entanglement between two oscillators in the same environment *Phys. Rev. Lett.* **100** 220401
[41] Jost J D, Home J P, Amini J M, Hanneke D, Ozeri R, Langer C, Bollinger J J, Leibfried D and Wineland D J 2009 Entangled mechanical oscillators *Nature* **459** 683
[42] Lü X-Y, Xiang Z-L, Cui W, You J Q and Nori F 2013 Quantum memory using a hybrid circuit with flux qubits and nitrogen-vacancy centers *Phys. Rev.* A **88** 012329
[43] Xiong H, Si L, Lv X, Yang X and Wu Y 2015 Review of cavity optomechanics in the weak-coupling regime: from linearization to intrinsic nonlinear interactions *Sci. China: Phys. Mech. Astron.* **58** 1
[44] Wang M, Lü X-Y, Wang Y-D, You J and Wu Y 2016 Macroscopic quantum entanglement in modulated optomechanics *Phys. Rev.* A **94** 053807
[45] Mancini S, Giovannetti V, Vitali D and Tombesi P 2002 Entangling macroscopic oscillators exploiting radiation pressure *Phys. Rev. Lett.* **88** 120401
[46] Vitali D, Mancini S and Tombesi P 2007 Stationary entanglement between two movable mirrors in a classically driven Fabry–Perot cavity *J. Phys. A: Math. Theor.* **40** 8055
[47] Liao J-Q, Wu Q-Q and Nori F 2014 Entangling two macroscopic mechanical mirrors in a two-cavity optomechanical system *Phys. Rev.* A **89** 014302
[48] Yang C-J, An J-H, Yang W and Li Y 2015 Generation of stable entanglement between two cavity mirrors by squeezed-reservoir engineering *Phys. Rev.* A **92** 062311
[49] Li J, Li G, Zippilli S, Vitali D and Zhang T 2017 Enhanced entanglement of two different mechanical resonators via coherent feedback *Phys. Rev.* A **95** 043819
[50] Vitali D, Gigan S, Ferreira A, Böhm H R, Tombesi P, Guerreiro A, Vedral V, Zeilinger A and Aspelmeyer M 2007 Optomechanical entanglement between a movable mirror and a cavity field *Phys. Rev. Lett.* **98** 030405
[51] Paternostro M, Vitali D, Gigan S, Kim M S, Brukner C, Eisert J and Aspelmeyer M 2007 Creating and probing multipartite macroscopic entanglement with light *Phys. Rev. Lett.* **99** 250401
[52] Zhou L, Han Y, Jing J and Zhang W 2011 Entanglement of nanomechanical oscillators and two-mode fields induced by atomic coherence *Phys. Rev.* A **83** 052117
[53] Ge W, Al-Amri M, Nha H and Zubairy M S 2013 Entanglement of movable mirrors in a correlated-emission laser *Phys. Rev.* A **88** 022338
[54] Ge W, Al-Amri M, Nha H and Zubairy M S 2013 Entanglement of movable mirrors in a correlated emission laser via cascade-driven coherence *Phys. Rev.* A **88** 052301
[55] Teklu B, Byrnes T and Khan F S 2018 Cavity-induced mirror-mirror entanglement in a single-atom Raman laser *Phys. Rev.* A **97** 023829
[56] Sete E A and Eleuch H 2015 Anomalous optical bistability and robust entanglement of mechanical oscillators using two-photon coherence *J. Opt. Soc. Am.* B **32** 971
[57] Luo D-W, Qian X-F and Yu T 2021 Nonlocal magnon entanglement generation in coupled hybrid cavity systems *Opt. Lett.* **46** 1073
[58] Wu W-J, Wang Y-P, Wu J-Z, Li J and You J Q 2021 Remote magnon entanglement between two massive ferrimagnetic spheres via cavity optomagnonics *Phys. Rev.* A **104** 023711
[59] Ren Y-L, Xie J-K, Li X-K, Ma S-L and Li F-L 2022 Long-range generation of a magnon-magnon entangled state *Phy. Rev.* B **105** 094422
[60] Kotler S *et al* 2021 Direct observation of deterministic macroscopic entanglement *Science* **372** 622
[61] Bhattacharya M, Giscard P-L and Meystre P 2008 Entanglement of a Laguerre-Gaussian cavity mode with a rotating mirror *Phys. Rev.* A **77** 013827
[62] Bhattacharya M, Giscard P-L and Meystre P 2008 Entangling the rovibrational modes of a macroscopic mirror using radiation pressure *Phys. Rev.* A **77** 030303
[63] Chen Z, Peng J-X, Fu J-J and Feng X-L 2019 Entanglement of two rotating mirrors coupled to a single Laguerre-Gaussian cavity mode *Opt. Express* **27** 29479
[64] Cheng H-J, Zhou S-J, Peng J-X, Kundu A, Li H-X, Jin L and Feng X-L 2021 Tripartite entanglement in a Laguerre–Gaussian rotational-cavity system with an yttrium iron garnet sphere *J. Opt. Soc. Am.* B **38** 285
[65] Singh S K, Peng J-X, Asjad M and Mazaheri M 2021 Entanglement and coherence in a hybrid Laguerre–Gaussian rotating cavity optomechanical system with two-level atoms *J. Phys. B: At. Mol. Opt. Phys.* B **54** 215502
[66] Pielawa S, Morigi G, Vitali D and Davidovich L 2007 Generation of Einstein-Podolsky-Rosen-entangled radiation through an atomic reservoir *Phys. Rev. Lett.* **98** 240401

[67] Cohen-Tannoudji C, Grynberg G and Dupont-Roe J 1992 *Atom-Photon Interactions* (New York: Wiley)
[68] Hu X 2015 Entanglement generation by dissipation in or beyond dark resonances *Phys. Rev.* A **92** 022329
[69] Walls D F and Milburn G J 2007 *Quantum Optics* (Berlin: Springer Science & Business Media)
[70] Scully M O and Zubairy M S 1997 *Quantum Optics* (Cambridge: Cambridge University Press)
[71] Aspelmeyer M, Kippenberg T J and Marquardt F 2014 Cavity optomechanics *Rev. Mod. Phys.* **86** 1391
[72] DeJesus E X and Kaufman C 1987 Routh-Hurwitz criterion in the examination of eigenvalues of a system of nonlinear ordinary differential equations *Phys. Rev.* A **35** 5288
[73] Vidal G and Werner R F 2002 Computable measure of entanglement *Phys. Rev.* A **65** 032314
[74] Adesso G, Serafini A and Illuminati F 2004 Extremal entanglement and mixedness in continuous variable systems *Phys. Rev.* A **70** 022318
[75] Parkins A S, Solano E and Cirac J I 2006 Unconditional two-mode squeezing of separated atomic ensembles *Phys. Rev. Lett.* **96** 053602
[76] Li L, Allen Y Y, Huang C, Grewell D A, Benatar A and Chen Y 2006 Fabrication of diffractive optics by use of slow tool servo diamond turning process *Opt. Eng.* **45** 113401
[77] Kaviani H, Ghobadi R, Behera B, Wu M, Hryciw A, Vo S, Fattal D and Barclay P 2020 Optomechanical detection of light with orbital angular momentum *Opt. Express* **28** 15482